Impermeable thin Al_2O_3 overlay for TBC protection from sulfate and vanadate attack in gas turbines

Quarterly Progress Report

Reporting Period Start Date: Mar. 01, 2003
Reporting Period End Date: May. 31, 2003
Principal Author: Scott X. Mao
Date Report was issued (Jun. 10, 2003)
DOE Award Number: DE-FC26-01NT41189

Department of Mechanical Engineering
University of Pittsburgh
3700 O'Hara St.
Pittsburgh, PA 15261
smao@engrng.pitt.edu, Tel: 412-624-9602

DISCLAIMER

ABSTRACT

In order to improve the hot corrosion resistance of yttria-stabilized zirconia (YSZ), an Al_2O_3 overlay has been deposited on the surface of YSZ by electron-beam physical vapor deposition. Currently, hot corrosion tests were performed on the YSZ coatings with and without Al_2O_3 overlay in molten salt mixture (Na_2SO_4 + 0~15wt%V_2O_5) at 950°C in order to investigate the effect of amount of vanadate on the hot corrosion behaviors. The results showed that the presence of in V_2O_5 the molten salt exacerbates the degradation of both the monolithic YSZ coating and the composite YSZ/Al_2O_3 system. The formation of low-melting Na_2O-V_2O_5-Al_2O_3 liquid phase is responsible for degradation of the Al_2O_3 overlay. The Al_2O_3 overlay acts as a barrier against the infiltration of the molten salt into the YSZ coating during exposure to the molten salt mixture with <5wt% vanadate.

In the next reporting period, we will use XPS and SIMS to study the interactions between alumina overlay and molten salt containing vanadate

TABLE OF CONTENTS

LIST OF GRAPHICAL MATERIALS

1. INTRODUCTION

Thermal-barrier coatings (TBCs), which consist of an yttria stabilized zirconia (YSZ) top-coating and an intermediate MCrAlY (M=Ni, Co, Fe) bond coating, are extensively used in gas turbines.[1-5] The application of TBCs can improve the durability of components and enhance the engine efficiency by increasing the turbine inlet combustion temperature. The common failure mode of TBC used in aviation gas turbines is that a thermally-growth oxide (TGO) forms and continuously grows between the top-coating and the bond coat. Because of the thermal expansion mismatch between the TGO and the bond coat, thermal cycling results in cracking, even spalling of TBCs.

TBCs are also finding increasing application in land-based industrial engines and sea engines which are usually operated with low quality fuels containing sulfur and vanadium.[5] In this case, another failure mode — hot corrosion become predominant and crucial to the lifetime of TBCs. During service, molten sulfate and vanadate salt condense on the TBCs at the temperature of 600-1000^{o}C.[6, 7] Although zirconia itself shows good resistance to the attack of the molten sulfate or vanadate compounds arising from fuel impurities, yttria is leached out of the zirconia by the reaction with V_2O_5 or $NaVO_3$ to form YVO_4, causing the structural destabilization of ZrO_2 (*i.e.*, transformation of the zirconia from the tetragonal and/or cubic to monoclinic phase). The structural destabilization of ZrO_2 is accompanied by a large destructive volume change, leading to large stresses within the YSZ, which eventually results in the delamination and spalling of the coating.[8-13]

Further improvement of engine efficiency requires TBCs being an integral part of the component which, in turn, desires reliable and predictable TBC performance. Hence, many methods have been developed to improve the hot corrosion resistant of TBCs to such harsh environment containing sulfate-vanadate deposits. For instance, based on Lewis acid-base concept, zirconias stabilized with india (In_2O_3),[14,15] scandia (Sc_2O_3)[16] and ceria (CeO_2)[11,17] as well as Ta_2O_5 [9, 18] and $YTaO_4$[18] have been evaluated for their hot corrosion resistance. On the other hand, over the years attempt has been made to seal the surface of zirconia TBCs by laser-glazing and arc lamp[19-21] or various "seal coats"[21-25] to prevent the penetration of molten deposits into the porous YSZ coating.

In the present work, a high-purity Al_2O_3 overlay is deposited onto the surface of YSZ coating by means of electron-beam physical vapor deposition (EB-PVD) technique in order to improve the hot corrosion resistance of TBCs. Alumina has a high melting point and stability without showing phase transition at high temperature like the ZrO_2 ceramics. Al_2O_3 has a small solubility particularly in molten salt and is expected to show an excellent corrosion resistance.[26] The hot corrosion tests of TiAl with Al_2O_3 coating in the sulfate melt at 900^{o}C have shown that the Al_2O_3 coating is very stable in the sulfate melt and effectively prevent the intermetallic TiAl from hot corrosion.[27] *Chen et al*'s experiment[28] has demonstrated that the Al_2O_3 coating could resist hot corrosion attack of molten Na_2SO_4 salt for longer time than the YSZ coating. In addition, Al_2O_3-ZrO_2 composite coatings have been explored as thermal barrier applications, showing better resistance in NaCl molten salt than YSZ.[29] This allows the potential application of Al_2O_3 in gas turbines.

In our study, both the monolithic YSZ coating and the composite YSZ/Al_2O_3 system will be exposed to the molten salt (Na_2SO_4+ 0~15wt%V_2O_5) at 950°C. The hot corrosion mechanism of the composite YSZ/Al_2O_3 system will be studied. The effect of the V_2O_5 content on the hot corrosion behavior of coatings will be investigated. The role of the Al_2O_3 in the hot corrosion resistance will be explored.

2. EXECUTIVE SUMMARY

The presence of V_2O_5 in the molten salt exacerbates the degradation of both the monolithic YSZ coating and the composite YSZ/Al_2O_3 system. The formation of low-melting Na_2O-V_2O_5-Al_2O_3 liquid phase is responsible for degradation of the Al_2O_3 overlay. The Al_2O_3 overlay acts as a barrier against the infiltration of the molten salt into the YSZ coating during exposure to the molten salt mixture with <5wt% vanadate.

3. EXPERIMENTAL

The TBC system used in the present work consisted of 6061 nickel-based superalloy substrate, CoNiCrAlY alloy bond coat as well as zirconia-8wt%yttira (YSZ) ceramic top coating. The 100 μm thick bond coating and the 200 μm thick YSZ were produced by low-pressure plasma spray (LPPS) and air plasma spray (APS), respectively.

The Al_2O_3 overlay was deposited by EB-PVD. The aluminum oxide coatings were deposited using an EB-PVD unit. Prior to deposition, the 1.5"x1.5" coupons were ultrasonically cleaned and dried. The vacuum unit was pumped down to a base pressure of 7.5 x 10^{-6} Torr with the oxygen gas lines being evacuated. Using two of the electron beams, the samples were preheated to ~1000°C and allowed to soak at 1000 °C for 20 minutes. During the evaporation of aluminum oxide, ~150 sccm of oxygen was flowed into the chamber to maintain the oxygen stoichiometry of the condensing coating (chamber pressure ~ 1x10^{-3} Torr). The average condensation rate was 0.88 μm/min. At the end of the desired deposition time, the samples were retracted into the load lock chamber and allowed to cool for 10 minutes with ~200 sccm of oxygen flow of before venting to atmosphere. The thickness of Al_2O_3 coating was approximately 25 μm.

Hot corrosion test was carried out on the TBCs with and without Al_2O_3 coating. The TBC plates were coated with a 150 mg cm^{-2} salt mixture (Na_2SO_4 + 0-15wt%V_2O_5) on a hot plate by dipping in a aqueous slurry of salt (1000 g / *l*), then placed carefully into a still air furnace, and isothermally held at 950°C for 10 hours. Melting of the salts mixture produced a thin liquid film on the surface of specimens. After exposure, the specimens were cooled down to room temperature in the furnace. The exposed specimens were cleaned in de-ionized water, resined in isoprypol alcohol and then dried. The Philips PW1700 X-ray diffractometer was then employed to analyze the corrosion products and phase transformation of ZrO_2 ceramic in the exposed samples.

The microstructure, composition of the coating surface and the cross-section were also examined using the PHILIPS XL30 scanning electron microscope (FE-SEM) equipped with an energy-dispersive spectrometer (EDS).

4. RESULTS AND DISCUSSION

4.1 XRD measurement

X-ray diffraction (XRD) analysis was performed on the coatings before and after hot corrosion testing. Pattern A in Fig.1 demonstrates that the T-phase of ZrO_2 was predominant in the monolithic YSZ coating before corrosion testing. After the monolithic YSZ coating was exposed to the molten salt of pure Na_2SO_4 at 950°C for 10 h, only a little amount of M-phase ZrO_2 was detected (Pattern B in Fig.1), and no chemical reaction was found. However, after exposure to the mixed molten salt of Na_2SO_4+5wt%V_2O_5, YVO_4 was formed (Pattern C in Fig.1), implying the leaching of Y_2O_3 from YSZ by the reaction of Y_2O_3 with V_2O_5. As a result, the intensity of T-phase decreased remarkably, and a considerable amount of M-phase was formed due to the leaching of Y_2O_3 from YSZ. As the V_2O_5 content in the molten salt mixture increased to 15wt%, much more M-phase ZrO_2 occurred in the coating after hot corrosion testing (Pattern D in Fig.1).

Fig.2 shows the XRD patterns of the composite YSZ/Al_2O_3 system before and after hot corrosion testing. The as-deposited Al_2O_3 overlay showed the γ-phase structure (Pattern A in Fig.2). As shown in Pattern B in Fig.2, there were no change in the structure of both the Al_2O_3 overlay and the YSZ layer after exposure to the pure Na_2SO_4 melt. In contrast, part of the γ-Al_2O_3 phase was transformed to α-Al_2O_3 phase after exposure to the mixed molten salt of Na_2SO_4+5wt.%V_2O_5 (Pattern C in Fig.2). Moreover, all the γ-Al_2O_3 phase was transformed to α-Al_2O_3 phase after exposure to mixed molten salt with 15wt.%V_2O_5 (Pattern D in Fig.2). It is well known that α-Al_2O_3 can only be produced by heating pure Al_2O_3 in air above 1200°C. This indicated that V_2O_5 played an important role in the phase transformation process from γ-Al_2O_3 to α-Al_2O_3 at 950°C. However, no evidence from the XRD patterns was found that the chemical reaction between the Al_2O_3 overlay and the molten salt had taken place. The results also showed that no YVO_4 peaks were present due to its low content that was below the detection limit of the XRD. The T-phase of ZrO_2 in the YSZ coating was still predominant and only a little amount of the M-phase of ZrO_2 existed in the YSZ coating after exposure to the molten salt of Na_2SO_4+5wt%V_2O_5. As demonstrated in pattern D in Fig.2, however, the amount of M-phase of ZrO_2 in the YSZ remarkably increased when the V_2O_5 content in the salt melt reached to 15wt%.

In order to evaluate the hot corrosion resistance of the TBCs with and without Al_2O_3 overlay, the extent of destabilization (*D*) of zirconia was estimated by

$$\mathrm{D}\ (\%) = \frac{M}{T+M} \times 100 \qquad (1)$$

Where *T* is the intensity of the zirconia tetragonal (111) peak, and *M* is the intensity of the ZrO_2 monoclinic $(11\bar{1})$ peak in XRD tests. Figure 3 shows the destabilization fraction of ZrO_2 (*D*%) after exposure to molten salts at 950°C for 10h. It can be seen from Fig.3 that both the

monolithic YSZ and the composite YSZ/Al_2O_3 system exhibited excellent resistance to hot corrosion in pure Na_2SO_4 melt, whereas the T-phase ZrO_2 in both the monolithic YSZ and the composite YSZ/Al_2O_3 system became destabilized during exposure to the mixed sulfate-vanadate salt. The destabilization fraction of ZrO_2 (*D%*) increased with increase in the V_2O_5 content in the molten salt mixture. The Al_2O_3 overlay had a significant effect on the destabilization fraction of ZrO_2. The destabilization fraction of ZrO_2 in the composite YSZ/Al_2O_3 system was about 8% after exposure to the mixed sulfate-vanadate salt with 5wt% V_2O_5. In contrast, the destabilization fraction of ZrO_2 in the monolithic YSZ coating reached up to 65%, indicating the penetration of molten salt into the YSZ through the pores and micro-cracks. The remarkable reduction of the destabilization fraction of ZrO_2 by the Al_2O_3 overlay indicated that the Al_2O_3 overlay acted a barrier against the penetration of molten into the YSZ layer. As the V_2O_5 content in salt was increased to 15wt%, the destabilization fraction of ZrO_2 in the composite YSZ/Al_2O_3 coating sharply reached up to 45%. This indicated that the Al_2O_3 overlay was no long a protective coating when exposed to the molten salt mixture containing high V_2O_5 content.

4.2 SEM observation

SEM examination was carried out on the surface of monolithic YSZ coating after 10h of exposure to the salt melt of Na_2SO_4+5wt%V_2O_5. And SEM microphotos exhibited many pyramid-like particles (Fig.4(a)). EDS analysis confirmed that the particles were rich in yttrium (40.53at%) and vanadium (36.31at%) and contained no zirconium. Keeping the XRD pattern in mind, these particles were identified to be YVO_4. The cross-section of the YSZ coating was examined as shown in Fig.4(b). YVO_4 was detected not only near the surface of YSZ but also in the area adjacent to the bond coat, implying that the molten salt was penetrated into the inner YSZ.

SEM observation of the surface of as-deposited Al_2O_3 overlay revealed a 'cauliflower' type of morphology (Fig.5(a)). It can be clearly seen from the SEM image of the cross-section that the Al_2O_3 overlay was dense and adherent to the porous YSZ coating (Fig.5(b)). The thickness of the Al_2O_3 coating was measured to be about 25μm. After exposure to the molten salt of pure Na_2SO_4, the surface of composite YSZ/Al_2O_3 system became dark green. Further SEM examination showed that the morphologies of the top surface and the cross-section showed little variation after exposure (Fig.6). The Al_2O_3 overlay was still dense and continuous.

After exposure to the molten salt mixture containing V_2O_5, visual examination showed that the surface became brown from white in color. Further SEM examination results are shown in Fig.7. Comparing Fig.7 with Fig.5 and Fig.6, it can be found that a significant change in the surface morphology of Al_2O_3 overlay took place after 10 h of exposure to the molten salt containing V_2O_5. Coarse acicular-shape α-Al_2O_3 crystals and faceted crystals were present, and the orientation of the crystals varied from region to region. Also, the preferential solution of grain boundaries occurred. About 97% of surface was still covered by Al_2O_3 overlay after exposure to molten Na_2SO_4+5wt%V_2O_5 salt (Fig.7(a)). However, after exposure to the molten Na_2SO_4+15wt%V_2O_5 salt, the YSZ was clearly visible on the surface, where Al_2O_3 was removed during corrosion exposure (Fig.7(b)).

Fig.8(a) demonstrates the cross-section of composite YSZ/Al_2O_3 system after 10 h of exposure to the molten salts of Na_2SO_4+5wt%V_2O_5. The Al_2O_3 overlay can be divided into two different regions. (i) The region close to the outer surface marked by "A" was bright and loose, which was corresponding to the acicular-shape α-Al_2O_3 crystals and faceted crystals (Fig.7(a)). (ii) The region adjacent to YSZ mraked by "B" was gray and relatively dense as compared with region "A". Because of the presence of dense layer "B", the attack of YSZ by the molten salt was arrested considerably (Fig.3). But some grooves existed within the region "B". It is worthy noting that the pores and cracks within the YSZ coating were filled with Al_2O_3 (indicated by arrows), which was confirmed by the EDS analysis as shown in Fig.8(b). And YVO_4 was also found in some pores and cracks within YSZ near the surface (Fig.8(c) and Fig.8(d)). In contrast, the pores and cracks within the YSZ coating before hot corrosion testing were empty (Fig.5(b)). Therefore, it is inferred that Al_2O_3 was absent in the YSZ coating before hot corrosion testing, and the presence of Al_2O_3 in the defects was caused by hot corrosion rather than by EP-PVD process.

Figure 9 illustrates the cross-section of composite YSZ/Al_2O_3 system after exposure to the molten salts of Na_2SO_4+15wt%V_2O_5. The integrated and dense Al_2O_3 overlay was no longer present, leaving separate α-Al_2O_3 fragments on the surface of YSZ, which was consistent with the surface micrograph (Fig.7(b)). Large Al_2O_3 pieces were "embedded" into the YSZ layer, leading to the interlacing of the Al_2O_3 layer with the YSZ layer at the interface. Owing to the absence of compact Al_2O_3 overlay on the surface of the YSZ, the YSZ layer was directly exposed to the molten salt. As a result, serious destabilization of ZrO_2 occurred during hot corrosion exposure (Fig.3).

4.3 Discussion

In agreement with previous studies,[3-11] the present work showed that YSZ was susceptible to the attack of sulfate-vanadate salt. Failure of the YSZ coating was ascribed to the infiltration of molten salt into the YSZ coating along pores and cracks in the YSZ and subsequent reaction of molten salt with Y_2O_3, leading to the destabilization of YSZ coating (Fig.3 and Fig.4). The degradation mechanism of YSZ was addressed in the previous investigations[3-11]. Therefore, the present study would focus on the hot corrosion mechanism of the composite YSZ/Al_2O_3 system.

(1) Hot corrosion in pure sulfate melt

Lawson et al have reported that intergranuluar corrosion can occur if an alumina-silicate phase existed along the grain boundaries of Al_2O_3 grains.[26] The preferential dissolution of grain boundary phase can be excluded in the present study because of the absence of the impurities along the grain boundaries. *Chen et al* have studied the hot corrosion behavior of the plasma-sprayed Al_2O_3 coating on the stainless steel when exposed in the molten Na_2SO_4 at 850°C.[28] They have found that Al_2O_3 reacted with molten Na_2SO_4 to form $NaAlO_2$. In the present investigation, however, no new corrosion products were detected by XRD and XPS after hot corrosion testing of the Al_2O_3 overlay in the molten salt of pure Na_2SO_4. In addition, the Al_2O_3 overlay did not show phase transformation and dissolution after exposure (Fig.1 and Fig.6).

At 950°C, there exists equilibrium for Na_2SO_4 melt as expressed by

$$Na_2SO_4 \rightarrow Na_2O + SO_3 \qquad (2)$$

$$\log a_{Na_2O} + \log P_{SO_3} = \frac{\Delta G^o(l)}{2.303RT} = -15.0 \qquad \text{(at 950°C [31])}$$

This melt exhibits acid/base chemistry, with Na_2O the basic component and SO_3 the acidic component. As shown by Eq.(1), as the activity of Na_2O, a_{Na_2O}, increases, the pressure of SO_3, P_{SO_3}, decreases and vice versa. During hot corrosion, the activity of Na_2O or the pressure of SO_3 in the molten salt determines the type and extent of reaction[32-34]. Hot corrosion may involve fluxing of oxides as either basic or acidic solutes in the molten salt. In case of the high Na_2O activity, alumina can react with Na_2O and dissolve in the molten sulfate by basic fluxing, which can be given by

$$Na_2SO_4\,(l) + Al_2O_3\,(s) \rightarrow 2NaAlO_2\,(l) + SO_3\,(g) \qquad (3)$$

In case of the low Na_2O activity and the correspondingly high P_{SO_3}, alumina can dissolve by acidic fluxing, which is shown by

$$Na_2SO_4\,(l) + Al_2O_3\,(s) \rightarrow Al_2(SO_4)_3\,(l) + SO_3\,(g) \qquad (4)$$

If the activity of Na_2O and the pressure of SO_3 are within the intermediate range, alumina is stable and negligible solubility in the molten sulfate occurs. Keep this in mind, it is not surprising that in our experiment no evident corrosion took place in the Al_2O_3 overlay.

(2) Hot corrosion in sulfate-vanadate melt

For the mixed sulfate-vanadate salt, V_2O_5 would be first melted upon heating due to its lower molting point (690°C). $NaVO_3$ could be formed by the reaction of molten Na_2SO_4 with V_2O_5 at the testing temperature of 950°C

$$Na_2SO_4\,(l) + V_2O_5\,(l) \rightarrow 2NaVO_3\,(l) + SO_3\,(g)$$

$$(?G^o = -11.9 \text{ kJ/mol at } 950°C) \qquad (5)$$

As a result, when YSZ/Al_2O_3 system was exposed to the Na_2SO_4+V_2O_5 salt melt, the $NaVO_3$-Na_2SO_4 melt covered the surface of the Al_2O_3 overlay. As reported in the previous literature,[33, 35] the presence of $NaVO_3$ increases the acidic solubility. Consequently, it is possible that metal oxides, such as Al_2O_3 and Y_2O_3, react with $NaVO_3$ to dissolve by acidic flux, which is expressed by

$$Al_2O_3\,(s) + 2NaVO_3\,(l) \rightarrow 2AlVO_4\,(l) + Na_2O\,(l) \qquad (6)$$

$$Y_2O_3\,(s) + 2NaVO_3\,(l) \rightarrow 2YVO_4\,(s) + Na_2O\,(l) \qquad (7)$$

However, $AlVO_4$ was not found in the composite Al_2O_3/YSZ coating that had been exposed to the molten sulfate-vanadate salt for 10 hours.

If we take a look at the phase diagram of $NaVO_3$-Al_2O_3 as shown in Fig.10,[36] we may find the reason for degradation of Al_2O_3 during exposure to the molten sulfate-vanadate salt. The $NaVO_3$-Al_2O_3 phase diagram demonstrates that a liquid phase containing Al, Na, V, and O will be formed when the temperature exceeds 610°C. Therefore, it is deduced that the formation of low-melting liquid phase was responsible for the failure of the Al_2O_3 overlay during hot corrosion testing. This notion can be confirmed by the further evidence in the present study. For instance, the surface of Al_2O_3 overlay exhibited a 'cauliflower' type of morphology before hot corrosion testing (Fig.5a), whereas the surface after hot corrosion testing was characteristic of

acicular-shape crystals and faceted crystals (Fig.7). In addition, the gap between the crystals was observed (Fig.7). In particular, the pores and cracks within the YSZ coating were filled with Al_2O_3 (Fig.8). This indicates that a liquid melt flowed along the pores and cracks.

When pure Al_2O_3 co-existed with $NaVO_3$ at 950ºC, a low-melting liquid phase containing Al, Na, V, and O was formed. The continuous formation of the liquid phase can result in loss of integrity of the surface. Upon cooling process, the liquid phase was then decomposed and Al_2O_3 crystallized to form acicular-shape crystals on the surface of the Al_2O_3 overlay (Fig.7). Keep this in mind, it was not surprising that the surface morphology of the overlay (region "A" in Fig.8(a)) was different from the subsurface region (region "B" in Fig.8(a)). Further attack by molten salt etched the subsurface region and caused the grooves. Then the liquid phase was infiltrated along the grooves and penetrated into pores and cracks within the YSZ coating. During cooling process, Al_2O_3 was crystallized from liquid phase and trapped in the pores and cracks within the YSZ coating. This was confirmed by SEM observation and EDS analysis as shown in Fig.8.

The solubility of Al_2O_3 in solvent $NaVO_3$ was estimated to be about 2.2 mol.% according to the phase diagrams.[36] When the molten salt contained only 5 wt%V_2O_5, the amount of alumina that could be dissolved by molten salt was limited due to limited V_2O_5 content. When the V_2O_5 content in the molten salt was increased to 15 wt%, however, more Al_2O_3 could be dissolved. Consequently, continuous formation of the liquid phase eventually resulted in loss of integrity of the surface and removal of dense alumina overlay. The outmost surface of YSZ could be fully covered by the liquid phase at 950°C. When this occurred, the Al_2O_3 overlay was no longer able to protect the inner YSZ layer. The liquid phase containing molten salts penetrated freely into the YSZ layer. As a result, significant M-phase of ZrO_2 was formed in this case. After cooling, Al_2O_3 was crystallized to form large α-Al_2O_3 acicular-shape crystals (Fig.7(b)).

In short, before corrosion exposure alumina exhibited the γ phase structure, which was thermodynamically metastable. During corrosion exposure, γ-Al_2O_3 was melted together with vanadate to form a liquid phase. After corrosion exposure, α-Al_2O_3, which was thermodynamically stable, was crystallized from the liquid phase upon cooling (Fig.2).

Dissolution of Al_2O_3 in molten salt depended on the V_2O_5 content in the mixture. In the current hot corrosion testing, the V_2O_5 content is much higher than that in real fuel (usually in the <100ppm range[37]). Although part of Al_2O_3 was degraded by the formation of low melting-point liquid phase, the Al_2O_3 overlay in the composite Al_2O_3/YSZ system acted as a barrier layer against the infiltration of the molten salt into the YSZ coating (as shown in Table 1). Destabilization of ZrO_2 was considerably restrained when the amount of V_2O_5 in the molten salt was less than 5wt% (Fig.3).

5. PLANS FOR THE NEXT REPORTING PERIOD

In the next reporting period, we will use XPS and SIMS to study the interactions between alumina overlay and molten salt containing vanadate

6. CONCLUSION

(1) Both the monolithic YSZ coating and the composite YSZ/Al_2O_3 system exhibited good hot corrosion resistance in the molten salt of pure Na_2SO_4.
(2) During exposure to the molten sulfate-vanadate salt mixture, the monolithic YSZ coating reacted with V_2O_5 to form YVO_4, leading to a significant structural destabilization of ZrO_2.
(3) Dissolution of Al_2O_3 in molten $NaVO_3$ was responsible for degradation of the Al_2O_3 overlay during hot corrosion testing. Degradation of the Al_2O_3 overlay was deteriorated with increase in the V_2O_5 content in the molten salt mixture.
(4) The Al_2O_3 overlay acted as a barrier against the infiltration of the molten salt into the YSZ coating when V_2O_5 content in salt was lower than about 5wt%. This restrained considerably the destabilization of ZrO_2.

7. REFERENCES

[1] M. J. Stiger, N. M. Yanar, M. G. Topping, F. S. Pettit, and G. H. Meier, "Thermal barrier coatings for the 21st century," *Z. Metallkd,* **90**[12] 1069-1078 (1999).

[2] L. Singheiser, R. Steinbrech, W.J. Quadakkers, R. Herzog, "Failure aspects of thermal barrier coatings", *Mat. High Temp*, **18** [4] 249-259 (2001)

[3] I. Gurrappa, "Hot corrosion of protective coatings," *Mat. Manuf. Process*, **15** [5]: 761-773 (2000).

[4] I. Gurrappa, "Thermal barrier coating for hot corrosion resistance of CM 247 LC superalloy," *J. Mater. Sci. Lett*. **17**, 1267-1269 (1998).

[5] R L. Jones, "Thermogravimetric study of the 800 degree reaction of zirconia stabilizing oxides with SO_3-$NaVO_3$," *J. Electrochem. Soc*., **139**, 2794-2799 (1992).

[6] K. L. Luthra, H. S. Spacil, "Impurity deposits in gas-turbines from fuels containing sodium and vanadium ," *J. Electrochem. Soc*., **129**[3] 649-656 (1982).

[7] N. S. Bornstein and W. P. Allen, "The chemistry of sulfidation corrosion - Revisited," *Mater. Sci. Forum*, **127,** 251-254 (1997).

[8] A. S. Nagelberg, "Destabilization of yttria-stabilized zirconia induced by molten sodium vanadate-sodium sulfate melts," *J. Electrochem. Soc.*, **132**[10] 2502-2507 (1985).

[9] R. L. Jones, C. E. Williams and S. R. Jones, "Reaction of vanadium compounds with ceramic oxides," *J. Electrochem. Soc.*, **133**[1] 227-230 (1986).

[10] R L. Jones, "High temperature vanadate corrosion of yttria-stabilized zirconia coatings on mild steel," *Surf. Coat. Tech.*, **37**, 271-284 (1989).

[11] R. L. Jones and C. E. Williams, "Hot corrosion studies of zirconia ceramics," *Surf. Coat. Tech.*, **32**, 349-358 (1987).

[12] D. W. Susnitzky, W. Hertl and C. B Carter, "Destabilization of zirconia thermal barriers in the presence of V_2O_5," *J. Am. Ceram. Soc*., **71**[11] 992-1004 (1988).

[13] R. A. Miller and C E. Lowell, "Failure mechanism of thermal barrier coatings exposed to elevated temperature," *Thin solid films*, **95**, 265-273 (1982).
[14] R. L. Jones, "India as a hot corrosion-resistant stabilizer for zirconia," *J. Am. Ceram. Soc*., **75** 1818-1821 (1992).
[15] R. L. Jones and R. F. Reidy, "Vanadate hot corrosion behavior of India, yttria-stabilized zirconia," *J. Am. Ceram. Soc*., **76**[10] 2660-2662 (1993).
[16] R. L. Jones, "Scandia-stabilized zirconia for resistance to molten vanadate-sulfate corrosion," *Surf. Coat. Tech.*, **39/40**, 89-96 (1989).
[17] S. A. Muqtader, R. K. Sidhu, E. Nagabhushan, K. Muzaffaruddin and S. G. Samdani, "Destabilization behavior of ceria-stabilized tetragonal zirconia polycrystals by sodium sulphate and vanadium oxide melts," *J. Mater .Sci. Lett*., **12**, 831-833 (1993).
[18] S. Raghavan and M J. Mayo, "The hot corrosion resistance of 20 mol% $YTaO_4$ stabilized tetragonal zirconia and 14 mol% Ta_2O_5 stabilized orthorhombic zirconia for thermal barrier coating applications," *Surf. Coat. Tech.*, **160**, 187-196 (2002).
[19] A. Petitbon, L. Boquet and D. Delsart, "Laser surface sealing and strengthening of zirconia coatings," *Surf. Coat. Tech.*, **49**, 57-61 (1991).
[20] Z. Liu, "Crack-free surface sealing of plasma sprayed ceramic coating using an excimer laser," *Appl. Surf. Sci.*, **186**, 135-139 (2002).
[21] S. Ahmaniemi, P. Vuoristo and T. Mantyla, "Improved sealing treatment for thick thermal barrier coatings," *Surf. Coat. Tech.*, **151-152**, 412-417 (2002).
[22] T. Mantyla, P. Vuoristo and P. Kettunen, "Chemical vapor deposition densification of plasma-sprayed oxide coatings," *Thin solid films*, **118**, 437-444 (1984).
[23] I. Berezin and T. Troczynski, "Surface modification of zirconia thermal barrier coatings," *J. Mater. Sci. Lett*., **15**, 214-218 (1996).
[24] T. Troczynski, Q. Yang and G. John, "Post-deposition treatment of zirconia thermal barrier coatings using sol-gel alumina," *J. Therm. Spray Tech.*, **8**(2), 229-234 (1999).
[25] M. Vippola, J. Vuorinen, P. Vuoristo, T. Lepisto and T. Mantyla, "Thermal analysis of plasma sprayed oxide coatings sealed with aluminum phosphate," *J. Euro. Ceram. Soc*., **22**, 1937-1946 (2002).
[26] M. G. Lawson, F. S. Pettit, J. R. Blachere, "Hot corrosion of Al_2O_3 ," *J. Mater. Res*., **8**, 1964-1971 (1993).
[27] Z. Tang, F. Wang, W. Wu, "Effect of Al_2O_3 and enamel coatings on 900^oC oxidation and hot corrosion behaviors of gamma-TiAl," *Mater. Sci. Eng. A*, **276**, 70-75 (2000).
[28] H. C. Chen, Z. Y. Liu, Y. C. Chuang, "Degradation of plasma-sprayed alumina and zirconia coatings on stainless steel during thermal cycling and hot corrosion," *Thin solid films*, **223**, 56-64 (1992).
[29] P. Ramaswamy, S. Seetharamu, K. B. R. Varma and K. J. Rao, "Al_2O_3-ZrO_2 composite coatings for thermal barrier applications," *Comp. Sci. Tech*., **57**, 81-89 (1997).
[30] J. Moulder, W. Stickle, P. Sobel, E. Bomben, *Handbook of X-ray photoelectron spectroscopy*, Physical Electronics, 1995.
[31] "JANAF Thermochemical Tables." 3d ed., *J. Phys. Chem. Ref. Data*, Suppl. **1**, 14 (1985).
[32] P. D. Jose, D. K. Gupta, R. Rapp, "solubility of α-Al_2O_3 in fused Na_2SO_4 at 1200K," *J. Electrochem. Soc.*, **132**[3] 735-737 (1985).

[33] R.A. Rapp, Y.S. Zhang, "Hot corrosion of materials: fundamental studies," *JOM*, **46**[12] 47-55 (1994).
[34] M. G. Lawson, H. R. Kim, F. S. Pettit, J. R. Blachere, "Hot corrosion of silica," *J. Am. Ceram. Soc.*, **73** [4] 989-995 (1990).
[35] Y. S. Hwang, R. R. Rapp, "Thermochemistry and solubilities of oxides in sodium sulfate-vanadate solutions," *Corrosion*, **45**[1] 933-937 (1989).
[36] L. A. Klinkova and E. A. Ukshe, "Solution of corundum in fused vanadates," *Russ. J. Inorg. Chem.*, **20** [2] 799-803 (1975).
[37] N S. Jacobson, "Corrosion of silicon-based ceramics in combustion environments," *J. Am. Ceram. Soc*., **76** [1] 3-28 (1993).

FIGURES

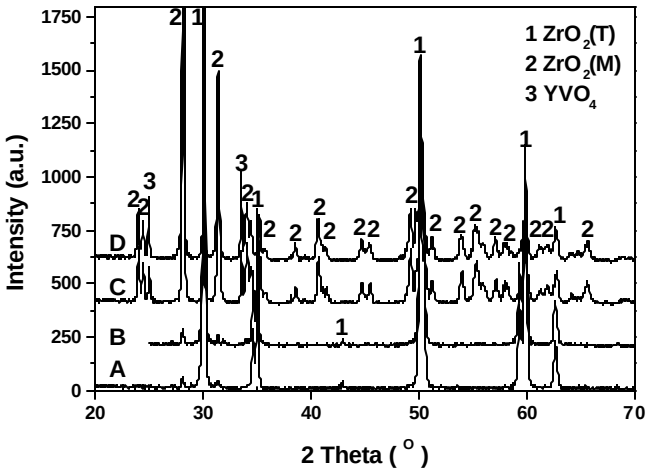

Fig.1 XRD patterns taken from the surface of the monolithic YSZ coating before and after 10 h of hot corrosion testing at 950°C. (Pattern A: before corrosion testing, Pattern B, C and D: after corrosion testing in Na_2SO_4, Na_2SO_4 +5wt.%V_2O_5 and Na_2SO_4 +15wt.%V_2O_5, respectively)

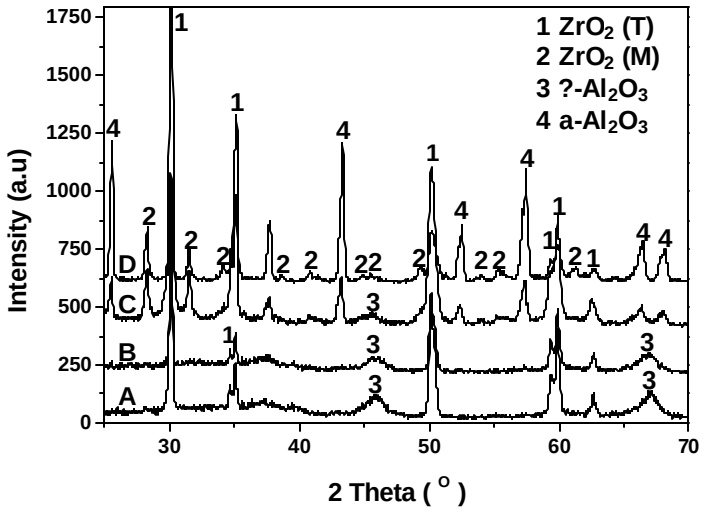

Fig.2 XRD patterns taken from the surface of composite YSZ/Al_2O_3 coating before and after 10 h of hot corrosion testing at 950°C (Pattern A: before corrosion testing, Pattern B, C and D: after corrosion testing in Na_2SO_4, Na_2SO_4 +5wt.%V_2O_5 and Na_2SO_4 +15wt.%V_2O_5, respectively)

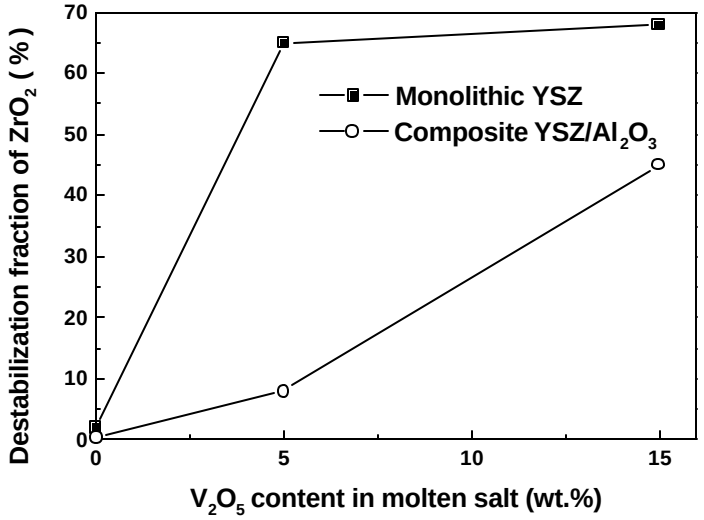

Fig.3 Destabilization fraction of zirconia in the YSZ layer as a function of V_2O_5 content in the molten salt after hot corrosion testing at 950°C for 10 h

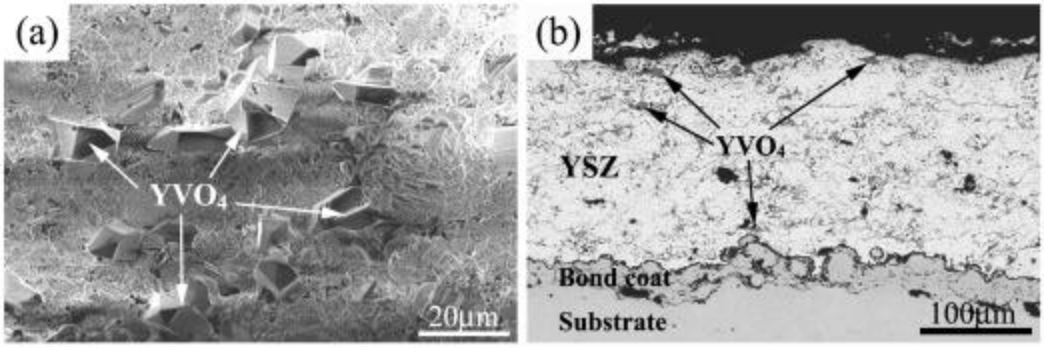

Fig.4 SEM images taken from the corroded TBC without Al_2O_3 overlay ((a) surface image, (b)cross-section image), showing the formation of YVO_4 after 10 h of corrosion testing at 950°C in salt melt of Na_2SO_4 + 5wt.%V_2O_5

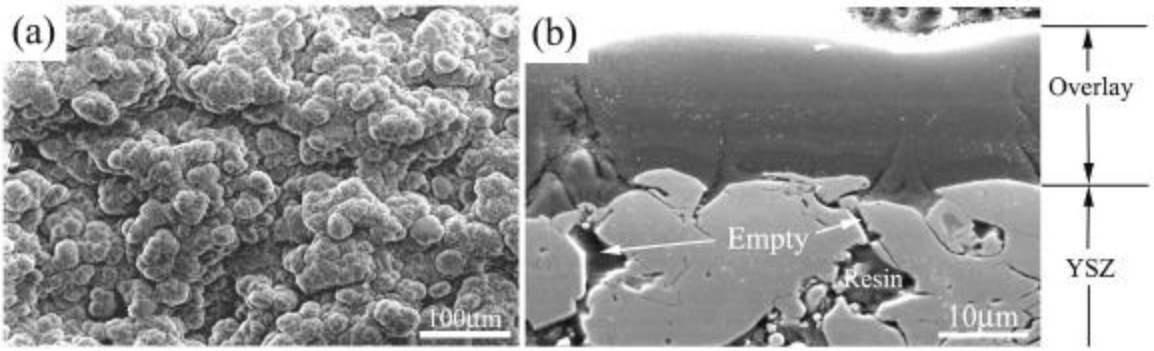

Fig.5 SEM photographs showing the surface of the Al_2O_3 overlay (a), and the cross-section of the YSZ/Al_2O_3 overlay (b)

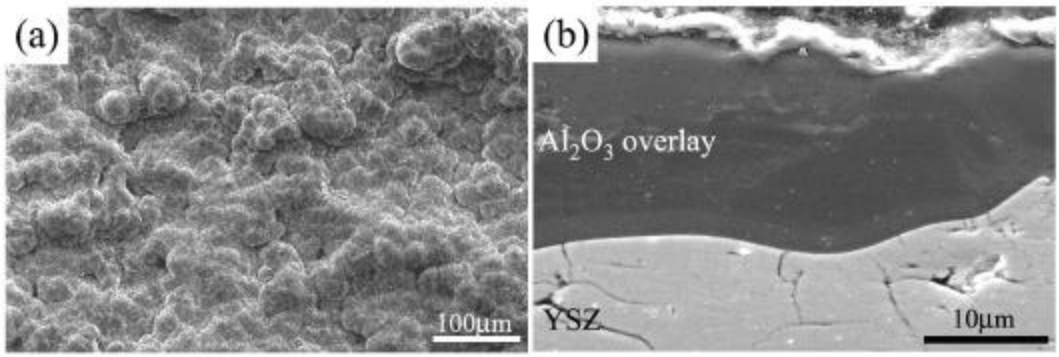

Fig.6 SEM images of YSZ with Al_2O_3 overlay after hot corrosion in molten Na_2SO_4 at 950°C for 10 h ((a)surface image, (b)cross-section image)

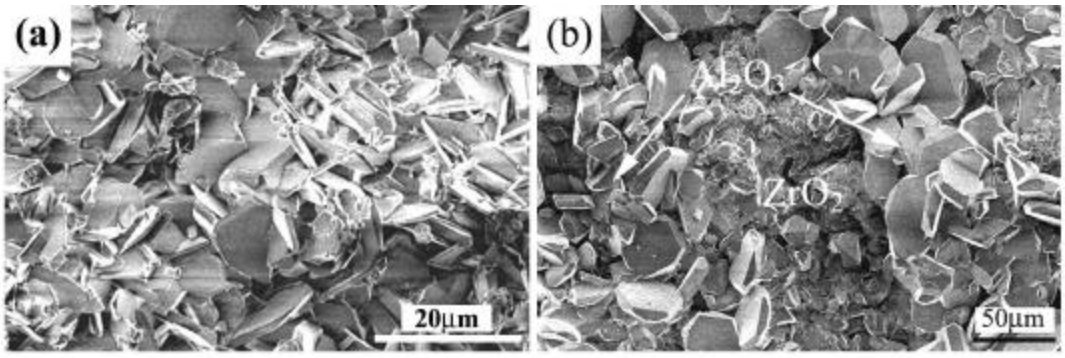

Fig.7 SEM photographs taken from the surface of composite YSZ/Al2O3 overlay after 10 h exposure at 950°C to the molten salts of (a) Na_2SO_4 +5wt.%V_2O_5 and (b) Na_2SO_4 +15wt.%V_2O_5

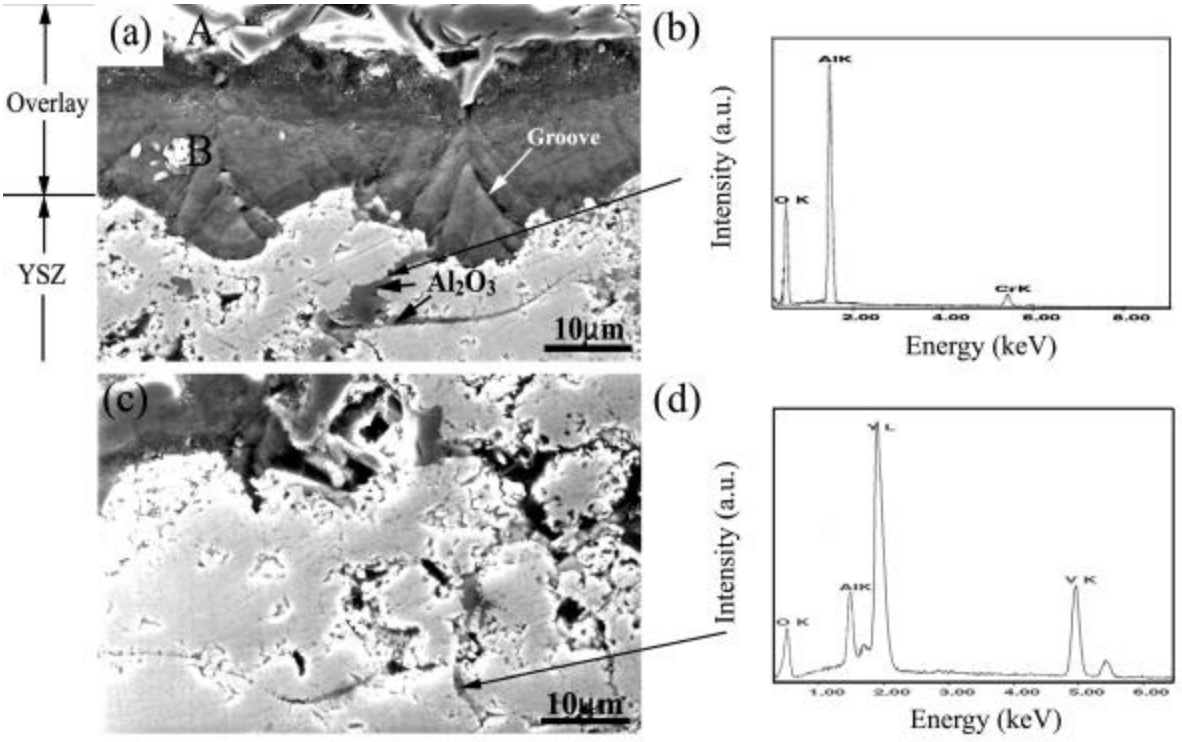

Fig.8 SEM photographs taken from the cross section of YSZ/Al_2O_3 overlay system. (a) the microstructure of composite YSZ/Al_2O_3 coating after 10 h exposure to the molten salt of Na_2SO_4 +5wt.%V_2O_5; (b) the EDS spectrum taken from the pores which indicated in Fig.8(a); (c) SEM photograph showing the filled cracks and pores; (d) the EDS spectrum taken from pores in Fig.8(c);

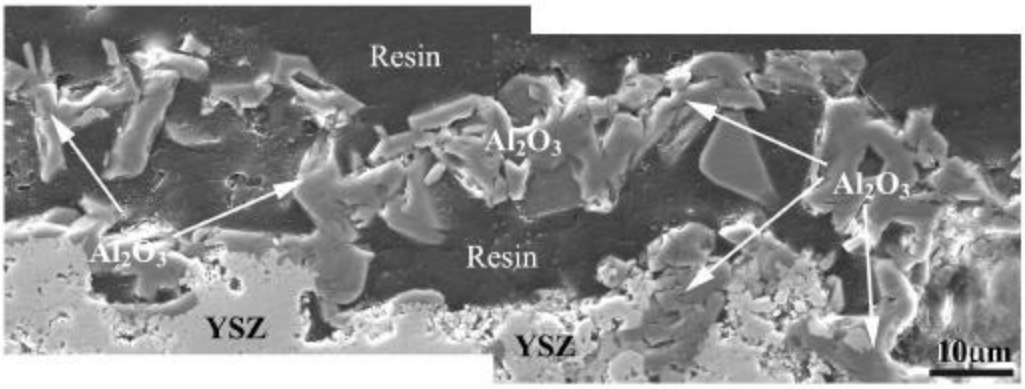

Fig.9 Cross section SEM photographs of YSZ/Al_2O_3 coating after 10 h of exposure at 950°C to the molten salt of Na_2SO_4 +15wt.%V_2O_5

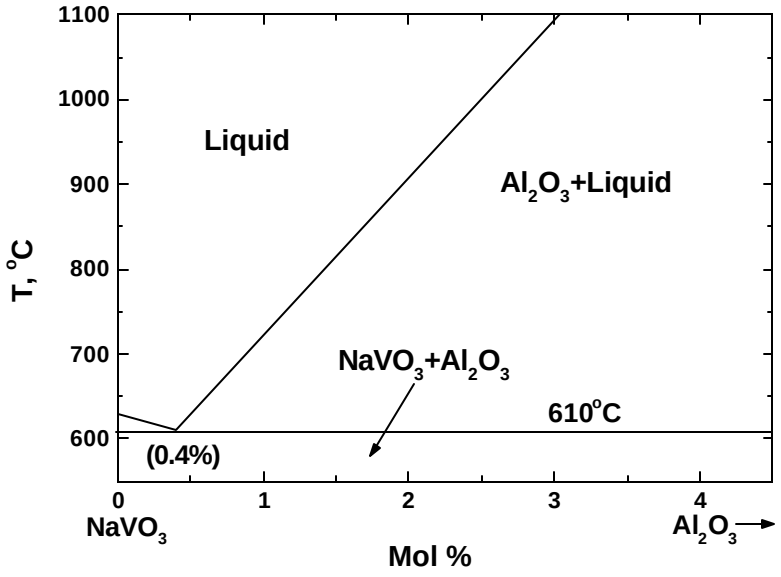

Fig.10 $NaVO_3$-Al_2O_3 Phase diagram showing the formation of liquid phase at the temperature above 610°C (After Klinkova and Ukshe.[36])